



## OPEN ACCESS

## EDITED BY

Volker Brüchert,  
Stockholm University, Sweden

## REVIEWED BY

Xiangjin Shen,  
Key Laboratory of Wetland Ecology and  
Environment, Northeast Institute of  
Geography and Agroecology, Chinese  
Academy of Sciences (CAS), China  
Sara Benelli,  
University of Parma, Italy

## \*CORRESPONDENCE

Wenzhi Cao,  
✉ wzcao@xmu.edu.cn

RECEIVED 11 March 2024

ACCEPTED 28 May 2024

PUBLISHED 16 July 2024

## CITATION

Zhang N, Dai Z, Wang F, Yang S and Cao W  
(2024), Geographical factor dominates spatial  
patterns of potential nitrate reduction rates in  
coastal wetland sediments in Fujian Province,  
China.

*Front. Earth Sci.* 12:1399200.

doi: 10.3389/feart.2024.1399200

## COPYRIGHT

© 2024 Zhang, Dai, Wang, Yang and Cao. This  
is an open-access article distributed under  
the terms of the [Creative Commons  
Attribution License \(CC BY\)](https://creativecommons.org/licenses/by/4.0/). The use,  
distribution or reproduction in other forums is  
permitted, provided the original author(s) and  
the copyright owner(s) are credited and that  
the original publication in this journal is cited,  
in accordance with accepted academic  
practice. No use, distribution or reproduction  
is permitted which does not comply with  
these terms.

# Geographical factor dominates spatial patterns of potential nitrate reduction rates in coastal wetland sediments in Fujian Province, China

Ning Zhang, Zetao Dai, Feifei Wang, Shengchang Yang and Wenzhi Cao\*

Key Laboratory of the Ministry of Education for Coastal Wetland Ecosystems, College of Environment and Ecology, Xiamen University, Xiamen, Fujian, China

Nitrate ( $\text{NO}_3^-$ ) reduction is a key process governing the nitrogen (N) dynamics of coastal wetland sediments. Although the effects of environmental factors on the  $\text{NO}_3^-$  reduction mechanism in coastal wetland sediments have been examined in various studies, the effects of spatial variation in potential  $\text{NO}_3^-$  reduction processes in coastal wetland sediments and the factors driving geographical variation in these processes have not been widely examined. Here, we conducted research on surface sediment samples from four different vegetation types at six coastal wetland sites across two regions. We characterized potential rates of  $\text{NO}_3^-$  reduction processes (including denitrification (DF), anammox (ANA), and dissimilatory nitrate reduction to ammonium (DNRA)) using a  $^{15}\text{N}$  tracer method. Additionally, we assessed the abundances of functional genes, and microbial community structure using high-throughput sequencing, and metagenomic sequencing. In six wetland sites, the contribution ranges of DF, ANA, and DNRA to  $\text{NO}_3^-$  reduction were 38.43%–55.69%, 31.33%–45.65%, and 5.26%–17.11%, respectively, and potential  $\text{NO}_3^-$  reduction was mainly driven by N removal via gaseous N (DF+ANA). Significant spatial differences were observed in the structure of bacterial and fungal microbial communities, suggesting that geographical distance has a major effect on microbial community structure. Environmental factors and Functional gene abundances were significantly related to potential  $\text{NO}_3^-$  reduction processes, and physicochemical properties had a stronger effect on potential  $\text{NO}_3^-$  reduction processes than gene abundances. Factors showing significant differences across regions were the main drivers of variation in potential  $\text{NO}_3^-$  reduction processes. Overall, our study showed that sediment substrates and geographical environmental factors rather than the abundance of functional genes and vegetation types were the main indicators of potential  $\text{NO}_3^-$  reduction activities in coastal wetlands.

## KEYWORDS

mangrove sediment, denitrification, anaerobic ammonium oxidation (anammox), dissimilatory nitrate reduction to ammonium (DNRA), geographical factors

## 1 Introduction

Fluxes of nutrients, especially nitrogen (N), into offshore areas have increased over the past century due to nutrient discharges derived from agricultural and industrial activities, as well as sewage treatment. N inputs from terrestrial ecosystems to coastal zones have doubled (Howarth et al., 2002; Galloway, 2005; Qu and Kroeze, 2010; Melillo, 2021; Kittu et al., 2023; Tian et al., 2023), and global N usage is projected to increase substantially by 2050 (Seitzinger et al., 2002; Vishwakarma et al., 2022). Mangrove ecosystems have high productivity and decomposition rates, and they are located at the ecotone of terrestrial and estuary ecosystems, which receive excess N and serve as hotspots of global N cycling (Lin, 1999; Kristensen et al., 2008). Variation in nutrient dynamics, especially N dynamics, has been documented in mangrove sediments worldwide (Reis et al., 2016; Alongi, 2018).

N in anaerobic mangrove sediments is mainly transformed through  $\text{NO}_3^-$  reduction processes such as denitrification (DF), anaerobic ammonium oxidation (ANA), and dissimilatory nitrate reduction to ammonium (DNRA) (Alkhatib et al., 2012). The first N removal pathway, DF, is present in nearly all ecosystems, and it can remove more than half of the N input from coastal and marine sediments (Pandey et al., 2020). The widespread ANA process very importantly removes both  $\text{NH}_4^+$ -N and  $\text{NO}_3^-$ -N from marine and estuarine sediments (Christensen, 1994). Overall, DF and ANA reduce N loading by mediating the conversion of  $\text{NO}_3^-$  to gaseous  $\text{N}_2$ . However, DNRA retains N as  $\text{NH}_4^+$ , which maintaining a relatively high N level in mangrove sediments (An and Gardner, 2002; Pandey et al., 2020). These processes are controlled by enzymes encoded by N functional genes (Kuypers et al., 2018). Generally, the main enzymes involved in DF process are the nitrate and nitrite reductases (encoded by the structural genes *narG*, *napAB*, *nirK* and *nirS*), nitric oxide reductases (encoded by genes *norBC* and *norZ*), and nitrous oxide ( $\text{N}_2\text{O}$ ) reductase (encoded by *nosZ*). The enzymes involved in ANA are the *hzs*, *hzo*, *hao* and *hh* genes. In contrast, in DNRA process, nitrite is reduced to ammonium by the enzyme encoded by *nrfA* and *nasA* gene. Consequently, molecular analyses of *nirS*, *nirK*, *nosZ*, *hzs*, *nrfA*, and *nasA* genes can be used to investigate the genetic potential of DF, ANA and DNRA process in environment (Dong et al., 2009; Luvizotto et al., 2019). However, previous studies have reported that gene abundances are not the main factors affecting N cycling (Li X. et al., 2019; Raes et al., 2020; She et al., 2023). Meta analysis showed that there was often no significant correlation between nitrogen cycling process and functional gene abundance due to the complexity of N cycling (Rocca et al., 2015). However, quantifying N transformation and abundance of related functional genes are still essential for a deeper understanding of the potential N cycling (Pandey et al., 2018).

In addition, the increase in human activities intensity can alter the partitioning of  $\text{N}_2$  production between nitrate reduction processes in estuarine sediments (Li et al., 2021). Due to the rapid economic development over the last four decades, most of the Chinese coastal waters have experienced an increase in N load (Wang et al., 2021), especially along the coast of Fujian Province (Wu et al., 2022). As an important ecological barrier, mangroves play an increasingly critical role in mitigating the increased N by rapid  $\text{NO}_3^-$  reduction processes. Nonetheless, the controlling factors

of the spatial distribution of potential  $\text{NO}_3^-$  reduction processes in mangrove sediments remain unclear. In this study, we assume that both environmental variables and functional genes of N cycling jointly control the spatial pattern of potential  $\text{NO}_3^-$  reduction processes in mangrove sediments, but which is dominant remains unclear. We investigated the potential  $\text{NO}_3^-$  reduction processes in surface sediments across six sampling sites, including mangrove sites dominated by three species and one salt marsh, in Zhangjiang Estuary and Shacheng Bay in Fujian Province. The aims of this study were to explore 1) the importance of N retention and removal in potential  $\text{NO}_3^-$  reduction processes in coastal wetland sediments; 2) variation in potential  $\text{NO}_3^-$  reduction processes among regions and vegetation types; and 3) the dominant factors affecting variation in potential  $\text{NO}_3^-$  reduction processes in coastal wetland sediments. We believe this research can deepen our understanding of N cycling in mangrove sediments, and provide scientific support for mangrove management.

## 2 Materials and methods

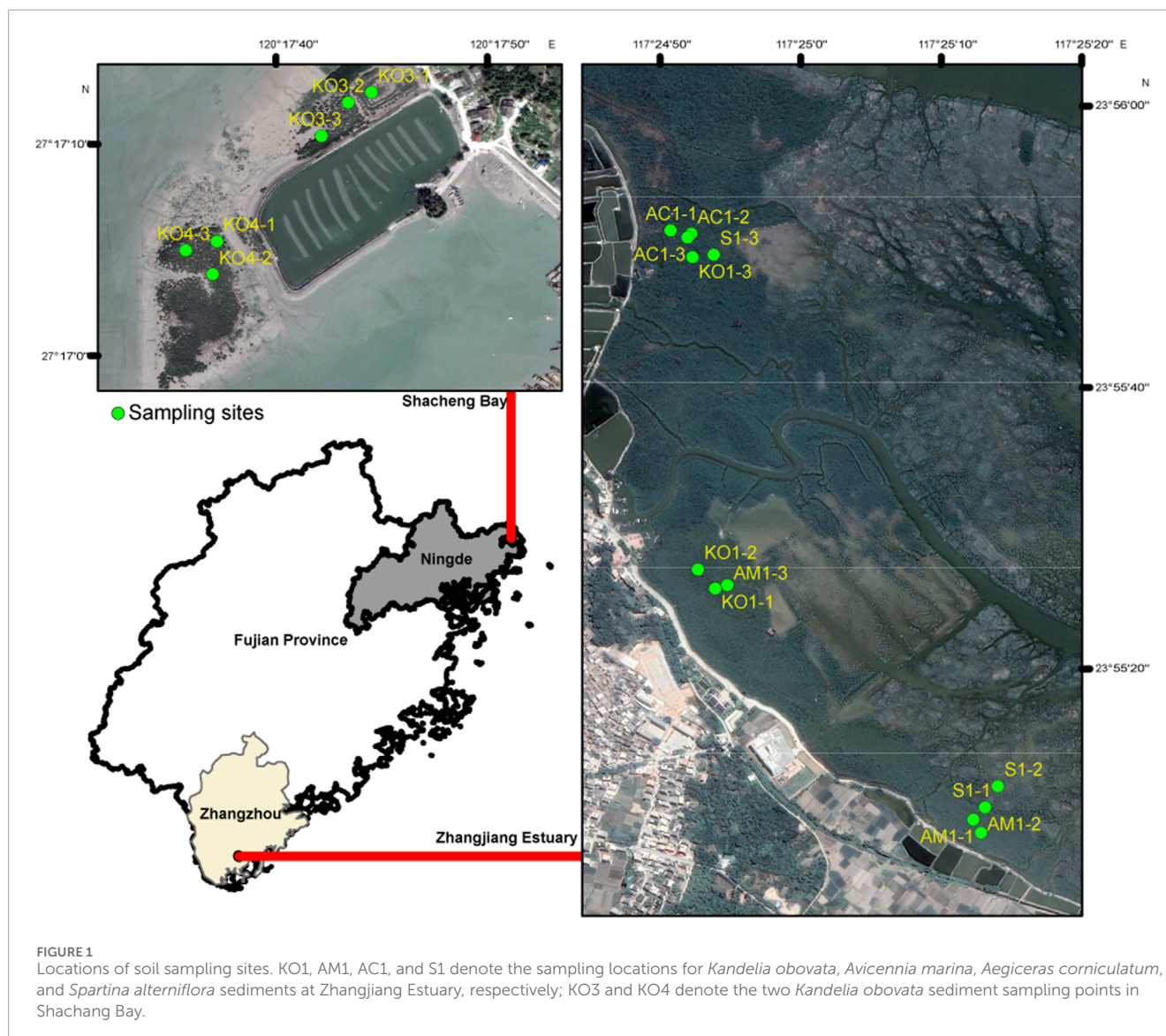
### 2.1 Field sites and sample collection

The Zhangjiang Estuary and Shacheng Bay are important mangrove distribution areas on the southern and northern sides of Fujian Province, respectively. There are geographical differences between the two areas. Shacheng Bay is the most northerly site where mangroves are known to be naturally distributed in China. Sampling in these two regions is conducive to investigating geographic variation in potential  $\text{NO}_3^-$  reduction processes in coastal wetland sediments.

Zhangjiang Estuary Mangrove National Nature Reserve (2,360  $\text{hm}^2$ ) is a typical coastal wetland ecosystem in Zhangzhou, Fujian Province (23°53'45"–23°56'00"N, 117°24'07"–117°30'00"E). The reserve experiences a subtropical maritime monsoon climate, with a mean annual temperature (MAT) of 21.2°C and a mean annual precipitation (MAP) of 1,679 mm. *Avicennia marina*, *Aegiceras corniculatum*, and *Kandelia obovata* are the dominant mangrove species in the reserve, and *Spartina alterniflora* was introduced to this reserve in the 1990s; it has since become common in tidal flats and mangrove margins.

Shacheng Bay is located in Ningde, Fujian Province (26°52'–27°26'N, 119°55'–120°43'E). Shacheng Bay experiences a subtropical maritime monsoon climate, with a MAT of 19.5°C and MAP of 1,686 mm. *K. obovata* is the only mangrove species in this area, and the heights of the mangrove trees range from 1.30 to 1.80 m; canopy closure is moderate and ranges from 40% to 69%.

Four distinct ecological communities, including *K. obovata* (KO1), *A. corniculatum* (AC1), *A. marina* (AM1), and *S. alterniflora* (S1), were sampled in Zhangjiang Estuary National Mangrove Forest Reserve, and two *K. obovata* communities (KO3 and KO4) were sampled in Shacheng Bay (Figure 1). Sediment sampling was conducted in December 2022. Triplicate 10- $\text{m}^2$  sample plots were randomly demarcated in each community, and three surface sediment samples (0–5 cm depth) were collected within each plots using the five-point sampling method (Chen et al., 2018). Each sample was immediately placed into a sterile plastic bag, and all samples were transported to the laboratory within 2 h of collection.



In the laboratory, all samples were divided into three parts: one part was stored at 4°C for analysis of physicochemical properties, the second part was used for slurry incubation, and the third part was frozen at -80°C for subsequent molecular analysis.

## 2.2 Sediment characterization

Sediment salinity (Sal) and pH were assessed using a WTW multiparameter meter (Multi 3630 IDS, WTW) after mixing ultrapure water with fresh sediment in a ratio of 2.5:1 (25 mL of water and 10 g of sediment). The water content (WC) was calculated based on sediment weight loss after drying at 105°C. Sediment ammonium ( $\text{NH}_4^+$ ), nitrite ( $\text{NO}_2^-$ ), and  $\text{NO}_3^-$  were measured using the potassium chloride (KCl) extraction method (40 mL of 2 M KCl solution and 8 g of sediment), and the nutrient concentrations were measured using a continuous flow analyzer (AutoAnalyzer 3, Bran+Luebbe GmbH) (Guan et al., 2018). Total carbon (TC), total nitrogen (TN), total sulfur (TS), and total organic

carbon (TOC) were measured using an Elemental Analyzer (2400 SERIES II CHNS/O, PerkinElmer) (Guo et al., 2024). Dissolved organic carbon (DOC) was determined using the potassium sulfate extraction method, and microbial biomass carbon (MBC) was measured using the chloroform fumigation-extraction method; analysis of DOC and MBC was performed using a TOC-VCPH elemental analyzer (TOC-VCPH, Shimadzu) (Guo et al., 2024). Easily oxidizable organic carbon (EOC) was quantified using the  $\text{KMnO}_4$  oxidation colorimetric method and analyzed using a spectrophotometer (DR3900, Hash) (Yang et al., 2022). The MAT and MAP were obtained from the National Science Meteorological Data Center (<https://data.cma.cn/>).

## 2.3 Measurement of microbial potential $\text{NO}_3^-$ reduction processes

Isotope experiments were carried out in an anaerobic glovebox filled with helium (He). Anoxic artificial seawater was prepared

through purged with He before adding sea salt in the anaerobic glovebox. Then, sediment slurries were prepared by mixing anoxic artificial seawater with fresh sediment at a 2:1 ratio (1,000 mL of water and 500 g of sediment) and preincubated anaerobically in the glovebox for 48 h to remove  $\text{NO}_3^-$ ,  $\text{NO}_2^-$  and oxygen in original sediment samples. After the preincubation, 20 mL samples were transferred into 120 mL crimp-top, serum vials. Then a  $\text{Na}^{15}\text{NO}_3$  solution was added to each pre-incubated vial (final concentration in slurry:  $100 \mu\text{mol L}^{-1}$  of  $^{15}\text{N-NO}_3^-$ ) before the vial was sealed (Canion et al., 2014; Pan et al., 2017; Sun et al., 2023). The isotope incubation experiment was set up with six sampling times after the addition of  $\text{Na}^{15}\text{NO}_3$  (0, 2, 4, 8, 12, and 24 h), with three replicates for each sampling time. During the incubation period, vials were shaking in a shaker with 150 rpm at temperature of  $25^\circ\text{C}$  in the dark (Zhang et al., 2020).

At sampling times during the incubation, vials were removed and shaken vigorously before extracting gas samples to ensure an equal distribution of gases between the dissolved and gaseous phases. Firstly, 1 mL of headspace gas of vial was taken used a microinjector and transferred to a 12 mL Labco bottle (Labco Limited, Lampeter, United Kingdom) filled with He. The  $^{30}\text{N}_2$  and  $^{29}\text{N}_2$  concentrations in Labco bottle were measured using an isotope ratio mass spectrometer system (GasBench II-Delta V Advantage system, Thermo Fisher Scientific, Bremen, Germany) with a  $\delta^{15}\text{N}$  accuracy of  $\pm 0.2\text{‰}$  (Cao et al., 2017). After gas sampling, the slurry was purged with He for 20 min to remove the dissolved  $^{30}\text{N}_2$  and  $^{29}\text{N}_2$ . Next,  $\text{NH}_4^+$  from slurry was extracted using a 2-M KCl solution and kept in a 12 mL Labco bottle. Then, the amount of  $^{15}\text{NH}_4^+-\text{N}$  produced was determined using the OX-MIMS method on Membrane Inlet Mass Spectrometer (MIMS; Bay Instruments, Easton, MD, United States) (Yin et al., 2014).

The potential rates of DF and ANA were calculated by the production rate of  $^{15}\text{N}_2$  (Thamdrup and Dalsgaard, 2002). The formulas were:

$$D_t = \frac{P_{30}}{F_N^2}$$

$$A_t = \frac{P_{29} + 2 \times \left(1 - \frac{1}{F_N}\right) \times P_{30}}{F_N}$$

$D_t$  represented the potential rate of DF;  $A_t$  represented the potential rate of ANA;  $P_{29}$  and  $P_{30}$  represented the production rates of  $^{29}\text{N}_2$  and  $^{30}\text{N}_2$ , respectively;  $F_N$  represented the  $^{15}\text{N}$  abundance of  $\text{NO}_3^-$  in slurry after adding of  $\text{Na}^{15}\text{NO}_3$ .

Potential DNRA rates were calculated by the production rate of  $^{15}\text{NH}_4^+$ . The formulas were:

$$\text{DNRA}_t = \frac{(\text{DN}) \times V}{W \times K}$$

$\text{DNRA}_t$  represented the potential rate of DNRA; DN represented the production rate of  $^{15}\text{NH}_4^+$  dissolved in water in the Labco bottle; V represented the volume of the Labco bottle; K represented the proportion of extraction solution; W represented the dry soil weight.

The N removal rate ( $R_{\text{N removal}}$ ) was defined as the sum of DF and ANA rates. The contribution rates of DF, ANA, and DNRA processes to  $\text{NO}_3^-$  reduction are DF%, ANA%, and DNRA%, respectively. The formulas were:

$$R_{\text{N removal}} = R_{\text{DF}} + R_{\text{ANA}}$$

$$\text{DF}\% = \frac{R_{\text{DF}}}{R_{\text{DF}} + R_{\text{ANA}} + R_{\text{DNRA}}} \times 100\%$$

$$\text{ANA}\% = \frac{R_{\text{ANA}}}{R_{\text{DF}} + R_{\text{ANA}} + R_{\text{DNRA}}} \times 100\%$$

$$\text{DNRA}\% = \frac{R_{\text{DNRA}}}{R_{\text{DF}} + R_{\text{ANA}} + R_{\text{DNRA}}} \times 100\%$$

$R_{\text{DF}}$ ,  $R_{\text{ANA}}$ , and  $R_{\text{DNRA}}$  represented the rates of DF, ANA, and DNRA, respectively.

## 2.4 Molecular analysis

Total genomic DNA was extracted using the CTAB method. Amplicons were extracted from 2% agarose gels. Specific primer pairs (341F-CCTAYGGGRBGCASCAG and 806R-GGACTACNNGGTATCTAAT) were used to amplify the V3-V4 regions of the bacterial 16S rRNA genes. Specific primer pairs (ITS1-F-CTTGGTCATTTAGAGGAAGTAA and ITS2-GCTGCGTTCATCGATGC) were also used to amplify the ITS1-ITS2 regions of the fungal 16S rRNA genes. Purification was carried out using an AxyPrep DNA Gel Extraction Kit (Axygen Biosciences, Union City, CA, United States), and quantification was performed using an ABI StepOnePlus Real-Time PCR System (Life Technologies, Foster City, United States). The library was sequenced on a NovaSeq 6000 PE250 platform (Illumina) that generated 250-bp paired-end reads. Raw data from the Illumina platform were filtered using FASTP (version 0.18.0), and clean OTUs obtained were clustered and denoised; species annotations for the OTUs were obtained using the SILVA and ITS2 databases.

Genomic DNA was extracted using the HiPure Bacterial DNA kit (Magen, Guangzhou, China). The quality of the extracted DNA was determined using a Qubit fluorometer (Thermo Fisher Scientific, Waltham, MA, United States) and Nanodrop spectrophotometer (Thermo Fisher Scientific, Waltham, MA). Qualified genomic DNA was fragmented to 350 bp by sonication. Both ends were flattened using enzymes, and an A-base was added to each end. A DNA library was obtained using the NEBNext MLtra DNA Library Prep Kits for Illumina (NEB, Ipswich, MA, United States) per the manufacturer's instructions. DNA fragments with lengths of 300–400 bp were enriched by PCR, and the amplified DNA fragments were purified using the AMPure XP system (Beckman Coulter, Brea, CA, United States). The size distribution of libraries was analyzed using a 2100 Bioanalyzer (Agilent, Santa Clara, CA, United States), followed by quantitative analysis using real-time PCR. Genome sequencing was performed on an Illumina NovaSeq 6000 sequencer (Illumina, Inc., San Diego, CA, United States) using the PE 150 sequencing strategy. Raw data from the Illumina platform were filtered using FASTP (version 0.18.0) by removing reads with 1)  $\geq 10\%$  unidentified nucleotides; 2)  $\geq 50\%$  bases with Phred quality scores  $\leq 20$ ; and 3) barcode adapters. After filtering, clean reads retained were used for genome assembly with the optimal k-mer and Megahit ver. 1.1.2. Gene prediction was performed on contigs  $>500$  bp using MetaGeneMark (ver. 3.38) (Qin et al., 2012; Feng et al., 2022; Zhao et al., 2023). The unigenes were annotated using DIAMOND (version 0.9.24) by aligning them with deposited sequences in different protein databases, including

the National Center for Biotechnology Information (NCBI) non-redundant protein database and the Kyoto Encyclopedia of Genes and Genomes (KEGG) (Song et al., 2022). Targeted N cycle-related genes were screened based on the major N-cycling pathways observed in all macrogenomic samples.

## 2.5 Statistical analyses

One-way analysis of variance (one-way ANOVA) was used to test for variability among the sediment characterization, potential rates of  $\text{NO}_3^-$  reduction processes, and functional gene abundances across different sites. Multiple comparisons were performed using the least significant difference and Student-Newman-Keuls tests following one-way ANOVA. Pearson correlation analysis and Redundancy analysis (RDA) was used to examine the relationships between potential  $\text{NO}_3^-$  reduction process rates, physicochemical properties, functional gene abundances, and climatic factors. The threshold for statistical significance in all tests was  $p < 0.05$ . These statistical tests were performed using SPSS 26 for Windows (IBM SPSS).

To evaluate microbial beta-diversity among samples, principal coordinate analysis based on the Bray-Curtis dissimilarity was performed using the “vegan” and “ape” packages (Xiao et al., 2022). We used analysis of similarity (ANOSIM) based on a Bray-Curtis dissimilarity matrix to evaluate differences among sampling sites (Yu et al., 2021). Graphs were plotted using the “ggplot2” package. All analyses were conducted in R version 4.3.2 (The R Project for Statistical Computing).

After screening the environmental factors significantly associated with potential rates of  $\text{NO}_3^-$  reduction processes according to Pearson correlation analysis, factors that exhibit significant differences between Zhangjiang Estuary and Shacheng Bay were classified as geo-environmental factors; the rest were classified as vegetation factors. We further investigated the pathway effects of potential  $\text{NO}_3^-$  reduction processes and the significant factors affected by spatial variables and vegetation types using a partial least squares-path model (PLS-PM), and non-parametric bootstrapping (1,000 resamples in this study) was used to estimate the precision of the PLS parameter estimates. The 95% bootstrap confidence interval was used to assess the significance of the estimated path coefficients; a path coefficient indicates the direction and strength of the direct effect between two variables. SmartPLS 3.2.9 (SmartPLS GmbH) was used to generate the PLS-PM (Li Y. et al., 2019; Bai et al., 2023).

## 3 Results

### 3.1 Characteristics and sediment properties

The physicochemical characteristics of sediments at all sites are shown in Figure 2. SWC was significantly lower in Shacheng Bay sediments than in Zhangjiang Estuary sediments ( $p < 0.05$ ). No significant variation in SWC was observed among the four communities in Zhangjiang Estuary ( $p > 0.05$ ). Sal was highest at KO1, and it was significantly higher at KO1 than at the other sampling sites ( $p < 0.05$ ). The Sal of Shacheng Bay sediments was

similar to that of AM1 sediments. With the exception of AC1, sediment samples were generally alkaline, with a pH range of 7.23–7.64. The sediment TC content varied considerably across communities; the TC content was highest at KO1, followed by AC1, AM1, S1, KO3, and KO4. The TC content was 2.03 times higher at KO1 than at the Shacheng Bay sites. The TN content was highest at AM1 and lowest at KO1.  $\text{NH}_4^+$  and  $\text{NO}_3^-$  were the primary components of inorganic N, and the content of  $\text{NO}_2^-$  was low. The inorganic N content was significantly lower at AC1 than at the other sites. Furthermore, the TS content was significantly higher at the Shacheng Bay sites than at the Zhangjiang Estuary sites ( $p < 0.05$ ).

### 3.2 Sediment potential $\text{NO}_3^-$ reduction rates

The potential DF rates in surface sediments (0–5 cm) varied considerably, ranging from 0.33 to 0.79  $\mu\text{mol N dry g}^{-1} \text{d}^{-1}$ , and the mean value was  $0.53 \pm 0.15 \mu\text{mol N dry g}^{-1} \text{d}^{-1}$ . The DF rate was significantly higher at AM1 than at the other sites ( $p < 0.05$ ). The ANA rates ranged from 0.32 to 0.61  $\mu\text{mol N dry g}^{-1} \text{d}^{-1}$ , and the average value was  $0.41 \pm 0.08 \mu\text{mol N dry g}^{-1} \text{d}^{-1}$ , which was slightly lower than the average DF rate. The ANA rate was highest at AC1 ( $p < 0.05$ ). The potential N removal rates from surface sediments ranged from 0.71 to 1.35  $\mu\text{mol N dry g}^{-1} \text{d}^{-1}$ , with a mean value of  $0.94 \pm 0.21 \mu\text{mol N dry g}^{-1} \text{d}^{-1}$ . The rate of N removal was markedly lower at the KO sites than at the other sites ( $p < 0.05$ ). The rates of DF, ANA, and N removal were similar at sites with the same vegetation type; however, there was notable spatial variation in the DNRA rate (Figure 3A).

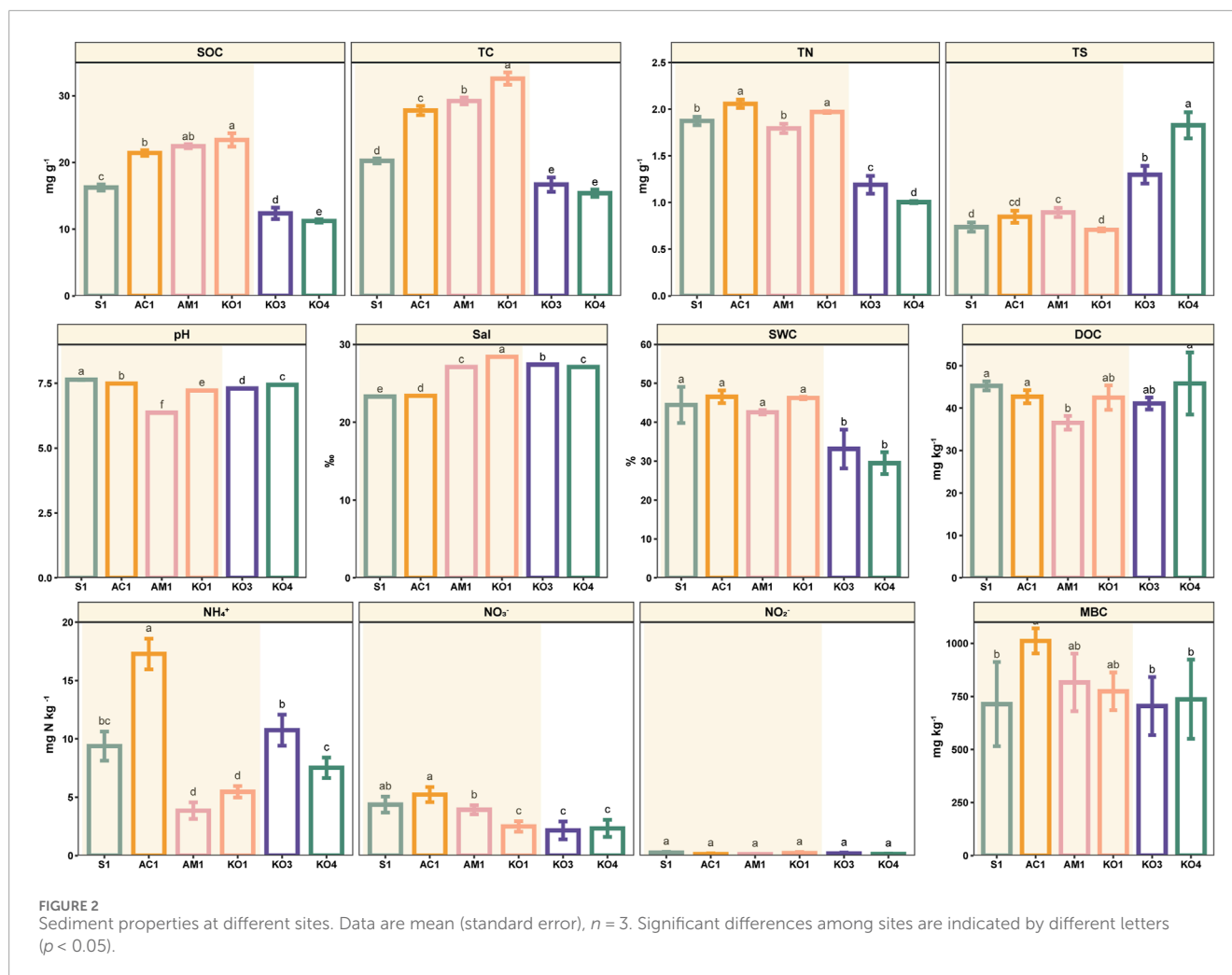
### 3.3 Functional gene abundances and microbial community structure

The primary genes involved in  $\text{NO}_3^-$  reduction processes were detected in the surface sediments. The highest relative abundance values of *hzs*, *nirS*, *nirK*, *nosZ*, *nrfA*, and *nasA* were 0.00079%, 0.096%, 2.16%, 1.96%, 0.018%, and 0.058%, respectively. The abundances of *nirK*, *nosZ*, *nrfA*, and *nasA* were highest at KO3 and lowest at KO4. The abundance of *hzs* was highest at AC1 and lowest at S1. The abundance of *nirS* was highest at AC1 and lowest at KO4 (Figure 3B).

Significant spatial variation was observed in the structure of bacterial and fungal microbial communities. Moreover, in Zhangjiang Estuary, fungal community structure in AM1 sediment significantly differed from that of the other sediment samples (Figure 4).

### 3.4 Relationship between potential $\text{NO}_3^-$ reduction processes and environmental factors

Correlation analyses between potential  $\text{NO}_3^-$  reduction rates, gene abundances, and environmental factors showed that DF was positively affected by sediment  $\text{NO}_3^-$  and negatively affected by MAP, Sal, and TC/ $\text{NO}_3^-$ . ANA was positively correlated with



SWC, MAT, TC, TN,  $\text{NH}_4^+$ ,  $\text{NO}_3^-$ , SOC, and MBC and negatively correlated with Latitude, MAP, and Sal. DNRA was negatively correlated with Latitude, MAP, and TS and positively correlated with SWC, MAT, TC, TN, SOC, and EOC. The abundance of *nirS* was positively correlated with TC, TN, SOC, EOC, and  $\text{NO}_3^-$  but negatively correlated with Latitude, MAP, and TS. DF was correlated with ANA and DNRA, but ANA was not correlated with DNRA. The abundance of *hzs* was positively correlated with TC, SOC, and EOC. The abundances of *nirK*, *nosZ*, *nrfA*, and *nasA* were not correlated with sediment physicochemical properties. The abundance of *nirS* was significantly correlated with DF, ANA, and DNRA, and the abundance of *hzs* was significantly correlated only with ANA. The abundance of *hzs* was only correlated with the abundance of *nirS*, and the abundances of the other genes were all correlated with each other, suggesting that gene abundances were affected by microbial biomass. In sum, Latitude, MAT, MAP, SWC, Sal, TC, TN,  $\text{NH}_4^+$ ,  $\text{NO}_3^-$ , SOC, EOC, MBC, TS,  $\text{TC}/\text{NO}_3^-$ , *hzs* gene abundance, and *nirS* gene abundance were the main factors affecting sediment potential  $\text{NO}_3^-$  reduction processes in coastal wetlands (Figure 5A).

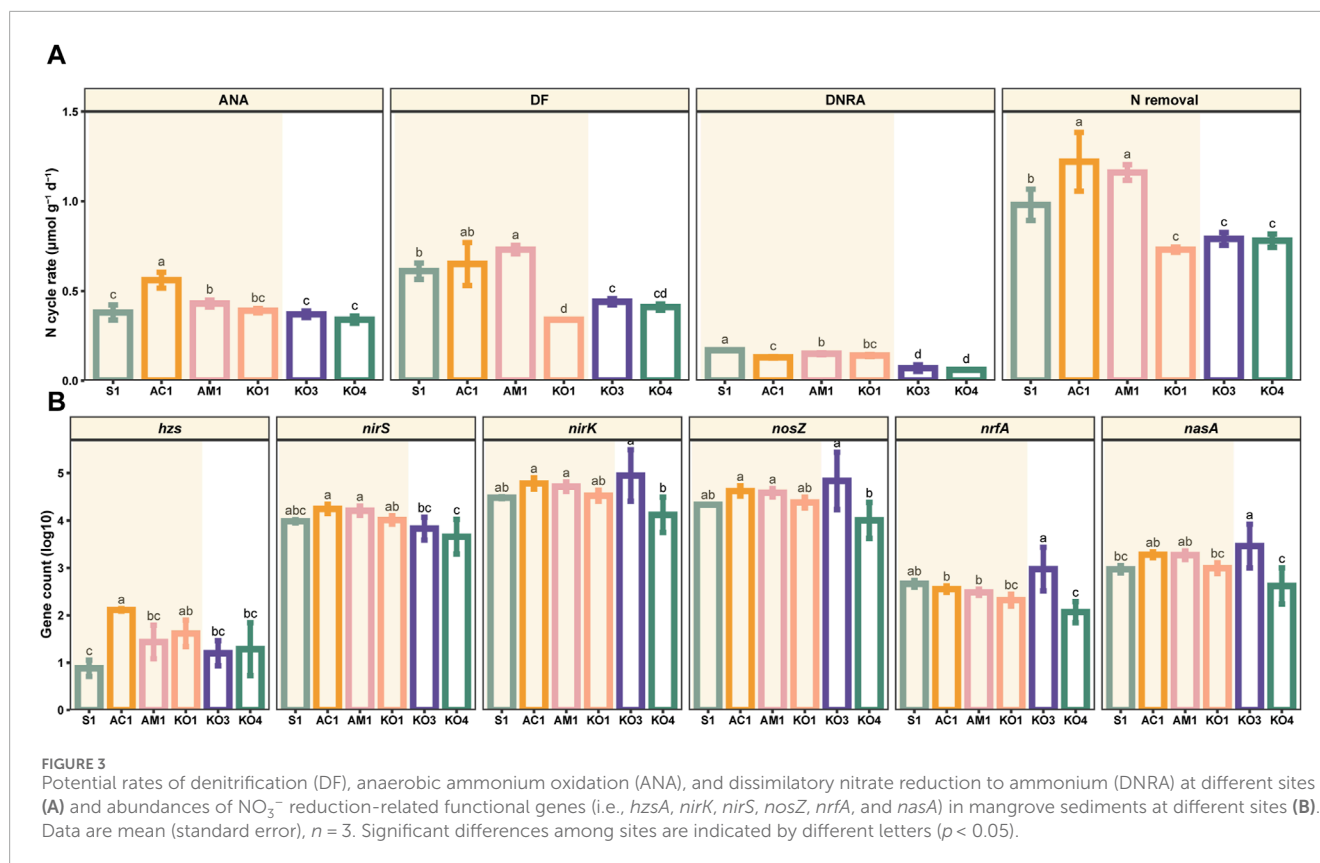
The RDA effectively explained the variation in the potential  $\text{NO}_3^-$  reduction process rates (Figure 5B). The *nrfA*, *nirK*, and *nasA* genes exhibited a high collinearity, and a strong correlation between the rates of potential DF and ANA was observed.

The PLS-PM model indicated that geo-environmental and vegetation factors could explain 87.0% of the variance in potential  $\text{NO}_3^-$  reduction rates. Potential  $\text{NO}_3^-$  reduction rates were positively affected by geo-environmental and vegetation factors, with path coefficients of 0.676 and 0.286, respectively. However, vegetation factors did not have a significant effect on potential  $\text{NO}_3^-$  reduction rates (Figure 5C).

## 4 Discussion

### 4.1 Climate and substrate were the main driver of system nitrogen fate

In the surficial sediment, the measured potential denitrification rates ( $0.33\text{--}0.79 \mu\text{mol N dry g}^{-1} \text{d}^{-1}$ , Figure 3A) and potential anammox rates ( $0.32\text{--}0.61 \mu\text{mol N dry g}^{-1} \text{d}^{-1}$ ) are comparable to those in other coastal sediments, but the potential rates of DNRA ( $0.05\text{--}0.17 \mu\text{mol N dry g}^{-1} \text{d}^{-1}$ ) observed in our study were lower than those documented in other mangroves (Table 1). Similar to other mangrove ecosystems, DF was the major pathway for potential  $\text{NO}_3^-$  reduction in the sediments of Zhangjiang Estuary



and Shacheng Bay (Tables 1, 2). Therefore,  $\text{NO}_3^-$  reduction generally led to N removal in coastal wetland sediments.

%DF, %ANA, and %DNRA were not affected by the abundance of related functional genes. Consistent with the results of a previous study (Hardison et al., 2015), TC/ $\text{NO}_3^-$  affected %DF and %ANA, as they were both affected by electron donors and substrates. The DNRA process showed greater sensitivity to temperature, with MAT having a positive effect on %DNRA, which is consistent with the findings of a previous study (Zhang et al., 2023). Moreover, %DNRA was positively correlated with sediment TC, TN, SOC, and EOC, suggesting that the substrate content also plays a key role in determining the rate of DNRA (Rahman et al., 2019). Our findings suggest that climatic factors such as MAT and MAP, as well as substrate factors such as TC/ $\text{NO}_3^-$ , TC, TN, SOC, and EOC affect the relative contributions of DF, ANA, and DNRA to  $\text{NO}_3^-$  reduction in coastal wetland sediments across the study area (Figure 5A).

## 4.2 Sediment nutrition rather than gene abundances drove nitrogen reduction across regions

Studies investigating the regulation of N fluxes in coastal ecosystems have highlighted the important role of sediment-dissolved inorganic nitrogen concentrations on  $\text{NO}_3^-$  reduction processes (Huang et al., 2021).  $\text{NO}_3^-$  is the substrate in  $\text{NO}_3^-$  reduction processes; therefore, its concentration in sediment affects the rates of different  $\text{NO}_3^-$  reduction pathways (Shan et al., 2018;

Tan et al., 2019; Rich et al., 2020). DF, ANA, and DNRA are microbial anaerobic respiration pathways that compete for  $\text{NO}_3^-$  in various natural habitats. Typically, DF and ANA rates exhibit a synergistic relationship (Figure 5A), which potentially stems from the provision of ANA with the  $\text{NO}_2^-$  substrate under anaerobic conditions by DF, as this has been commonly observed in laboratory environments (You et al., 2020). Furthermore, studies conducted in different ecosystems have shown that the most important factor affecting DF and DNRA rates is TC/ $\text{NO}_3^-$ , rather than TC or  $\text{NO}_3^-$  content alone (Pandey et al., 2018; Pandey et al., 2019; Bai et al., 2020). Likewise, some studies also found that the dominant N reduction process shifted from DNRA to DF process with the decreasing values of TC/ $\text{NO}_3^-$  (Figure 5A) (Yoon et al., 2015; Van Den Berg et al., 2016; Pandey et al., 2018).

The effect of environmental factors on the potential  $\text{NO}_3^-$  reduction process might vary across geographic scales. In contrast to heterotrophic DF (Saggar et al., 2013), autotrophic ANA has traditionally been considered independent of sediment carbon (C) or organic C (Kartal et al., 2013; Shan et al., 2018; Huang et al., 2022). However, studies from regional and global perspectives have revealed a positive correlation between ANA rates and the soil C and N content, including TOC and TN (Yao et al., 2023), which is consistent with the findings of this study. In coastal sediments, environments with a high C-to-N ratio amplify the substrate competition between DF and ANA (Li et al., 2022), which explains why DF rates were higher than ANA rates (Brin et al., 2017) (Figures 3A, 5A).

Potential  $\text{NO}_3^-$  reduction processes may be affected by various factors across different geographic scales. Studies in

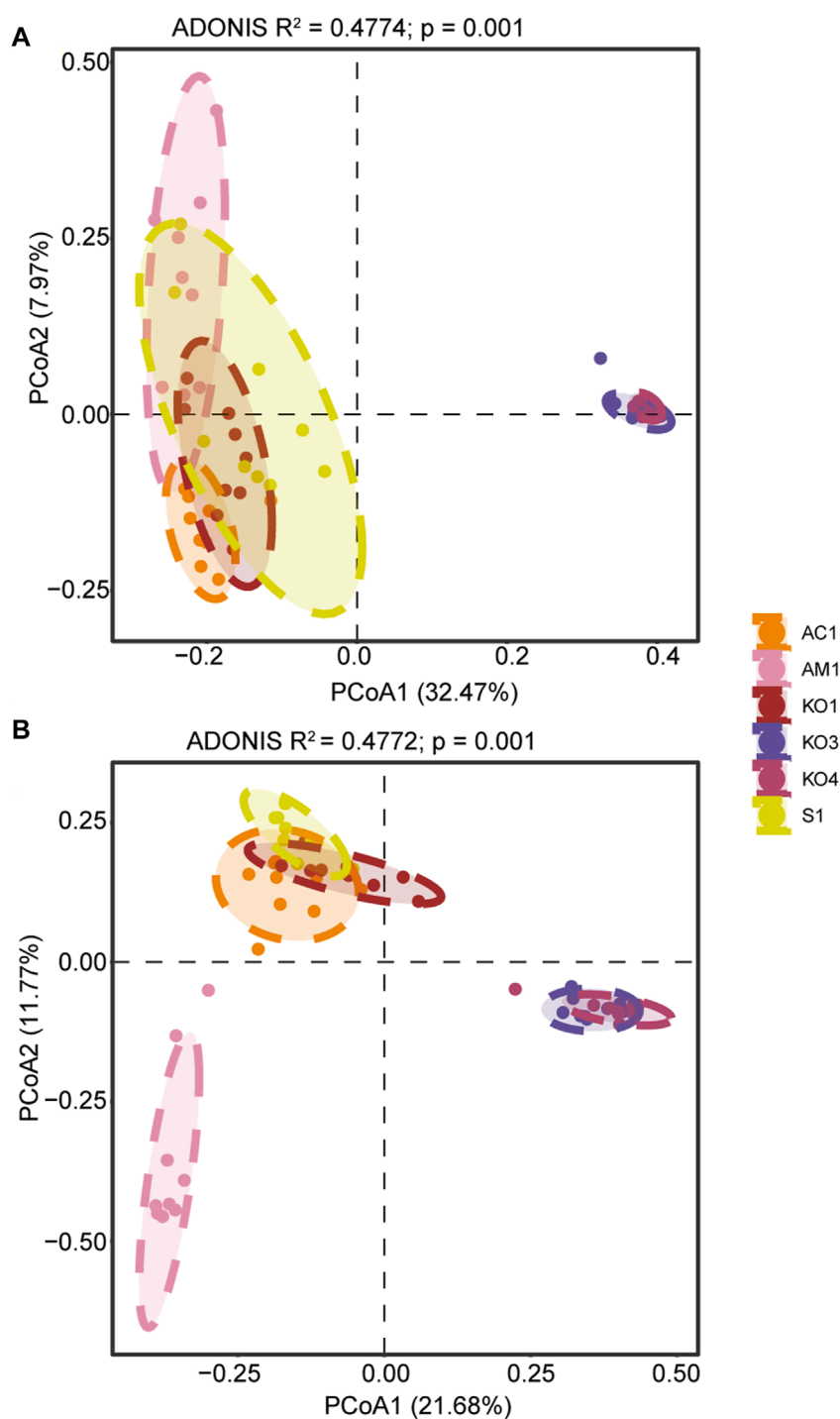


**FIGURE 4**  
Results of principal coordinate analyses (PCoA) of (A) bacterial and (B) fungal community structure.

regions with low environmental complexity suggest that DF, ANA, and DNRA rates are mainly regulated by the abundances of functional genes, followed by environmental factors (Jiang et al., 2023). Conversely, studies in regions with greater environmental complexity indicate that these potential  $\text{NO}_3^-$  reduction rates are mainly controlled by physicochemical properties, such as substrate availability (Shrewsbury et al., 2016; Raes et al., 2020; She et al., 2023). In these studies, the sampling sites exhibited a huge difference

in the degree of human influence (such as types of pollution sources and land uses) and natural conditions (including latitude, MAT, and MAP). In our study, the DF rate was only significantly correlated with the abundance of *nirS* genes, whereas ANA was significantly correlated with the abundances of *hzs* and *nirS*. The DNRA rate was not correlated with the abundance of *nrfA* (Figure 5A). On the one hand, the expression of N functional genes is affected by sediment physicochemical properties (Carbone et al., 2011; Ahmed et al.,

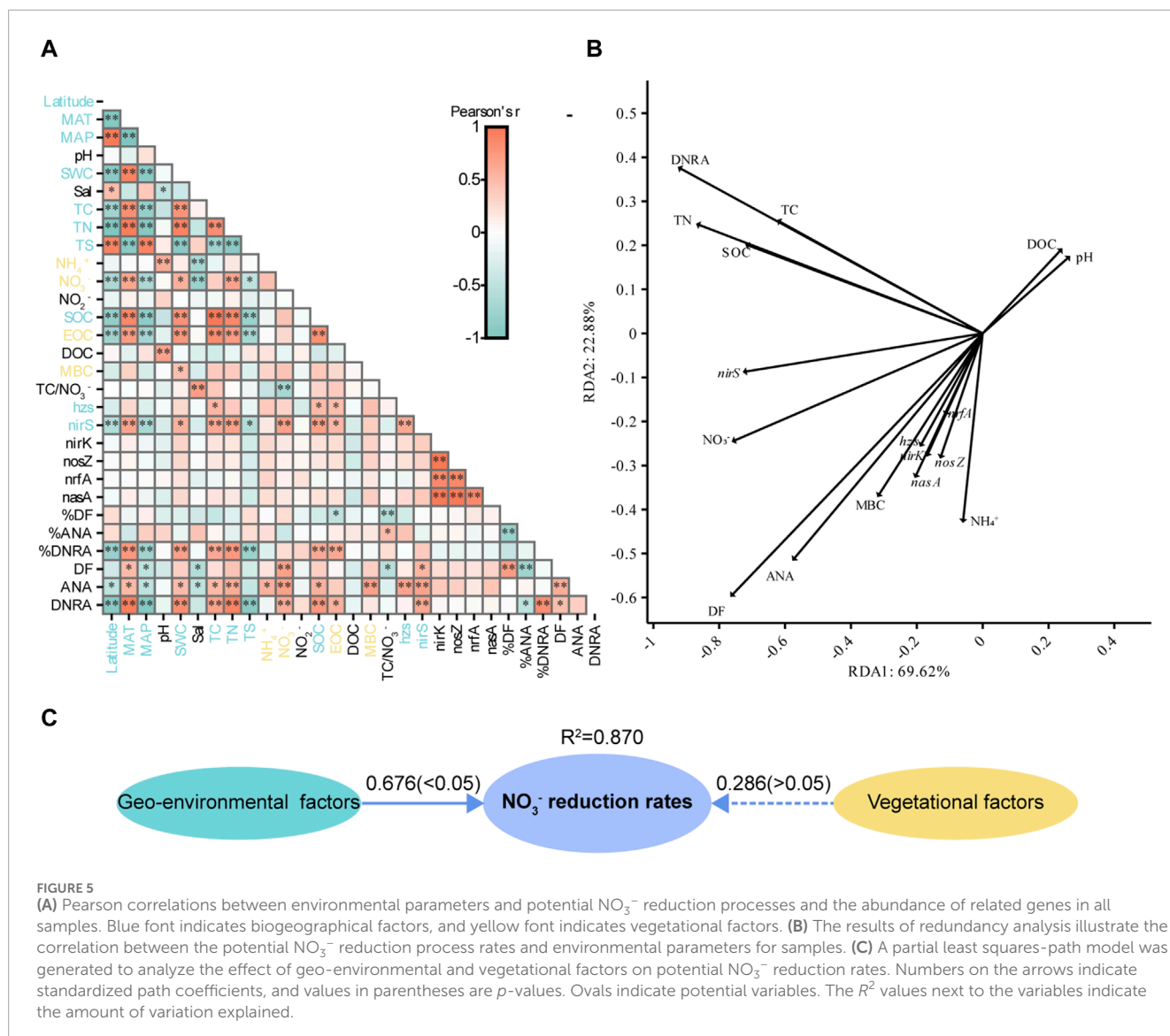


**TABLE 1** Previous reported NO<sub>3</sub><sup>-</sup> reduction rates in mangrove sediments (Fernandes et al., 2012; Molnar et al., 2013; Cao et al., 2016; Luvizotto et al., 2019; Fang et al., 2022; Wang and Lin, 2023).

Site	Rates (nmol N g <sup>-1</sup> h <sup>-1</sup> )		
	Denitrification	Anammox	DNRA
Tuvem	30 (1.15)	4 (0.0012)	891 (23)
Divar	64 (1.15)	4 (10)	500 (13)
Bertioga	11,940 (710)	340 (540)	1,350 (190)
Jiulongjiang Estuary	3.5 (0.76)	2.1 (2.3)	39 (9.2)
Zhangjiangkou Estuary	5.7 (0.5)	1.3 (0.085)	5.8 (0.48)
Q'iao Island	3.81 (0.47)	0.21 (0.09)	2.41 (0.48)
New Caledonia	0.98 (0.39)	ND	0.91 (0.45)

Data are mean (standard error), *n* = 3; ND, means no data; When the original data unit is rate per square meter and the sediment properties are not specified in the paper, the unit conversion is based on a surface layer of 5 cm, a bulk density of 1.5 g cm<sup>-3</sup>, and a water content of 70%.

TABLE 2 Contribution ratio of  $\text{NO}_3^-$  reduction process.

Site	%DF (%)	%ANA (%)	%DNRA (%)
AC1	48.38 (4.36)	41.81 (3.39)	9.81 (1.2)
AM1	55.52 (0.28)	33.17 (0.29)	11.31 (0.04)
KO1	38.83 (0.4)	44.74 (0.82)	16.43 (0.61)
S1	52.76 (0.16)	32.68 (1.18)	14.56 (1.04)
KO3	49.83 (1.25)	42.52 (0.93)	7.65 (2.08)
KO4	51.09 (0.34)	41.97 (0.43)	6.94 (0.09)

Data is the mean (standard error),  $n = 3$ .

2018; Huang et al., 2021). On the other hand, the relative importance of various factors regulating the structure of microbial communities might vary across spatial scales (Martiny et al., 2006; Hazard et al., 2013; Xu et al., 2016). Complex habitats lead to differences in microbial community structure (Figure 4), and the expression efficiency of functional genes also changed with the structure of microbial communities (Nogales et al., 2002; Dandie et al., 2011). Furthermore, the abundance of functional genes is not influenced by physicochemical properties (Figures 5A, B). Therefore, establishing a direct relationship between gene abundances and potential  $\text{NO}_3^-$  reduction rates across various habitats remains a major challenge. The findings suggested that potential  $\text{NO}_3^-$  reduction activities in coastal sediments across regional scales were more strongly affected by sediment substrates than by gene abundances.

### 4.3 Geographical environmental factors dominated spatial patterns in nitrogen reduction

Coastal wetlands exhibited various physicochemical properties across geographic regions (Shen et al., 2021; La et al., 2022). Additionally, differences in plant species contribute to variation in depositional conditions and physicochemical properties in the understory sediments (Chen and Twilley, 1999; Nie et al., 2021). Among the environmental factors that were significantly associated with potential  $\text{NO}_3^-$  reduction process rates, the value of Latitude, MAT, MAP, SWC, SOC, TC, TN, TS, *hzs* gene abundance, and *nirS* gene abundance significantly differed between sediment samples from Zhangjiang Estuary and Shacheng Bay (Figure 2). However, there were significant differences in EOC, MBC,  $\text{NH}_4^+$ , and  $\text{NO}_3^-$  among different vegetation types. In this study, geo-environmental factors were found having a stronger effect on potential  $\text{NO}_3^-$  reduction processes than vegetation factors (Figure 5C), indicating that geo-environmental factors were the main drivers of potential  $\text{NO}_3^-$  reduction processes in coastal sediments at the regional scale rather than vegetation factors.

In addition, hydrological conditions may be an important influencing factor in the nitrogen reduction process (Wang et al., 2019; Deng et al., 2020; Kaden et al., 2021). N storage, N cycling processes, and N fluxes have a unique distribution pattern along hydrological gradients in intertidal zone, while future changes in hydrological conditions will also lead to a transition from  $\text{NH}_4^+$

sources to sinks of intertidal ecosystems (Hu et al., 2019). The impact is likely achieved by regulating the nutrient supply (Hu et al., 2019; Kaden et al., 2021) and dissolved oxygen levels in sediments (Abbas et al., 2019; Gao et al., 2022) in sediments. However, during laboratory incubation, the changes in hydrological conditions are not taken into account.

## 5 Conclusion

The results of our study reveal the environmental determinants that affect the potential  $\text{NO}_3^-$  reduction process in coastal sediments, as well as the effects of regional and vegetation-related factors on potential  $\text{NO}_3^-$  reduction activities in coastal sediments across regional scales. Potential  $\text{NO}_3^-$  reduction processes in coastal sediments were predominantly affected by sediment substrates at the regional scale. However, the expression of functional genes was decoupled from the potential  $\text{NO}_3^-$  reduction processes due to the effects of variation in sediment properties and microbial community structure. Moreover, factors showing regional differences primarily contributed to variation in the potential rates of  $\text{NO}_3^-$  reduction. The results of this study indicated that geo-environmental factors play a major role in shaping spatial variation in potential  $\text{NO}_3^-$  reduction in coastal wetland sediments. These findings have important implications for future studies of the N cycling process in sediments across various regions.

## Data availability statement

The data presented in the study are deposited in the China National Microbiology Data Center (NMDC) repository, accession number NMDC10018760: <https://nmdc.cn/resource/en/genomics/project/detail/NMDC10018760>.

## Author contributions

NZ: Writing—original draft, Data curation, Methodology. ZD: Writing—original draft, Data curation. FW: Visualization, Writing—review and editing. SY: Writing—review and editing. WC: Writing—review and editing, Conceptualization, Funding acquisition, Project administration.

## Funding

The author(s) declare that financial support was received for the research, authorship, and/or publication of this article. This research was supported by the National Natural Science Foundation of China (No. 42230407) and the National Key Research and Development Program of China (No. 2022YFF1301301).

## Conflict of interest

The authors declare that the research was conducted in the absence of any commercial or financial relationships that could be construed as a potential conflict of interest.

## Publisher's note

All claims expressed in this article are solely those of the authors and do not necessarily represent those of their affiliated

organizations, or those of the publisher, the editors and the reviewers. Any product that may be evaluated in this article, or claim that may be made by its manufacturer, is not guaranteed or endorsed by the publisher.

## References

- Abbas, T., Zhang, Q., Jin, H., Li, Y., Liang, Y., Di, H., et al. (2019). Anammox microbial community and activity changes in response to water and dissolved oxygen managements in a paddy-wheat soil of Southern China. *Sci. total Environ.* 672, 305–313. doi:10.1016/j.scitotenv.2019.03.392
- Ahmed, M. A., Sanaullah, M., Blagodatskaya, E., Mason-Jones, K., Jawad, H., Kuzyakov, Y., et al. (2018). Soil microorganisms exhibit enzymatic and priming response to root mucilage under drought. *Soil Biol. Biochem.* 116, 410–418. doi:10.1016/j.soilbio.2017.10.041
- Alkhatib, M., Lehmann, M. F., and del Giorgio, P. A. (2012). The nitrogen isotope effect of benthic remineralization-nitrification-denitrification coupling in an estuarine environment. *Biogeosciences* 9 (5), 1633–1646. doi:10.5194/bg-9-1633-2012
- Alongi, D. (2018). Impact of global change on nutrient dynamics in mangrove forests. *Forests* 9 (10), 596. doi:10.3390/f9100596
- An, S. M., and Gardner, W. S. (2002). Dissimilatory nitrate reduction to ammonium (DNRA) as a nitrogen link, versus denitrification as a sink in a shallow estuary (Laguna Madre/Baffin Bay, Texas). *Mar. Ecol. Prog. Ser.* 237, 41–50. doi:10.3354/meps237041
- Bai, R., Fang, Y.-T., Mo, L.-Y., Shen, J.-P., Song, L.-L., Wang, Y.-Q., et al. (2020). Greater promotion of DNRA rates and nrfA gene transcriptional activity by straw incorporation in alkaline than in acidic paddy soils. *Soil Ecol. Lett.* 2, 255–267. doi:10.1007/s42832-020-0050-6
- Bai, X., Li, Y., Jing, X., Zhao, X., and Zhao, P. (2023). Response mechanisms of bacterial communities and nitrogen cycle functional genes in millet rhizosphere soil to chromium stress. *Front. Microbiol.* 14, 1116535. doi:10.3389/fmicb.2023.1116535
- Brin, L. D., Giblin, A. E., and Rich, J. J. (2017). Similar temperature responses suggest future climate warming will not alter partitioning between denitrification and anammox in temperate marine sediments. *Glob. Change Biol.* 23 (1), 331–340. doi:10.1111/gcb.13370
- Canion, A., Kostka, J. E., Gihring, T. M., Huettel, M., van Beusekom, J. E. E., Gao, H., et al. (2014). Temperature response of denitrification and anammox reveals the adaptation of microbial communities to *in situ* temperatures in permeable marine sediments that span 50° in latitude. *Biogeosciences* 11 (2), 309–320. doi:10.5194/bg-11-309-2014
- Cao, W., Guan, Q., Li, Y., Wang, M., and Liu, B. (2017). The contribution of denitrification and anaerobic ammonium oxidation to N<sub>2</sub> production in mangrove sediments in Southeast China. *J. Soils Sediments* 17 (6), 1767–1776. doi:10.1007/s11368-017-1653-0
- Cao, W., Yang, J., Li, Y., Liu, B., Wang, F., and Chang, C. (2016). Dissimilatory nitrate reduction to ammonium conserves nitrogen in anthropogenically affected subtropical mangrove sediments in Southeast China. *Mar. Pollut. Bull.* 110 (1), 155–161. doi:10.1016/j.marpolbul.2016.06.068
- Carbone, M. S., Still, C. J., Ambrose, A. R., Dawson, T. E., Williams, A. P., Boot, C. M., et al. (2011). Seasonal and episodic moisture controls on plant and microbial contributions to soil respiration. *Oecologia* 167 (1), 265–278. doi:10.1007/s00442-011-1975-3
- Chen, R., and Twilley, R. R. (1999). Patterns of mangrove forest structure and soil nutrient dynamics along the shark river estuary, Florida. *Estuaries* 22 (4), 955–970. doi:10.2307/1353075
- Chen, Y., Jiang, Y., Huang, H., Mou, L., Ru, J., Zhao, J., et al. (2018). Long-term and high-concentration heavy-metal contamination strongly influences the microbiome and functional genes in Yellow River sediments. *Sci. Total Environ.* 637–638, 1400–1412. doi:10.1016/j.scitotenv.2018.05.109
- Christensen, J. P. (1994). Carbon export from continental shelves, denitrification and atmospheric carbon dioxide. *Cont. Shelf Res.* 14 (5), 547–576. doi:10.1016/0278-4343(94)90103-1
- Dandic, C. E., Wertz, S., Leclair, C. L., Goyer, C., Burton, D. L., Patten, C. L., et al. (2011). Abundance, diversity and functional gene expression of denitrifier communities in adjacent riparian and agricultural zones. *FEMS Microbiol. Ecol.* 77 (1), 69–82. doi:10.1111/j.1574-6941.2011.01084.x
- Deng, D., Pan, Y., Liu, G., Liu, W., and Ma, L. (2020). Seeking the hotspots of nitrogen removal: a comparison of sediment denitrification rate and denitrifier abundance among wetland types with different hydrological conditions. *Sci. Total Environ.* 737, 140253. doi:10.1016/j.scitotenv.2020.140253
- Dong, L. F., Smith, C. J., Pappaspyrou, S., Stott, A., Osborn, A. M., and Nedwell, D. B. (2009). Changes in benthic denitrification, nitrate ammonification, and anammox process rates and nitrate and nitrite reductase gene abundances along an estuarine nutrient gradient (the Colne estuary, United Kingdom). *Appl. Environ. Microbiol.* 75 (10), 3171–3179. doi:10.1128/AEM.02511-08
- Fang, X., Yang, Z., and Han, J. (2022). The relative dominance of denitrification and dissimilatory nitrate reduction to ammonium (DNRA) under four vegetation types in a typical coastal wetland. *Appl. Soil Ecol.* 177, 104528. doi:10.1016/j.apsoil.2022.104528
- Feng, L., Zhang, Y., Liu, W., Du, D., Jiang, W., Wang, Z., et al. (2022). Effects of heat stress on 16S rDNA, metagenome and metabolome in Holstein cows at different growth stages. *Sci. Data* 9 (1), 644. doi:10.1038/s41597-022-01777-6
- Fernandes, S. O., Bonin, P. C., Michotey, V. D., Garcia, N., and LokaBharathi, P. A. (2012). Nitrogen-limited mangrove ecosystems conserve N through dissimilatory nitrate reduction to ammonium. *Sci. Rep.* 2, 419. doi:10.1038/srep00419
- Galloway, J. N. (2005). The global nitrogen cycle: past, present and future. *Sci. China Ser. C-Life Sci.* 48, 669–678. doi:10.1007/bf03187108
- Gao, D., Liu, C., Li, X., Zheng, Y., Dong, H., Liang, X., et al. (2022). High importance of coupled nitrification-denitrification for nitrogen removal in a large periodically low-oxygen estuary. *Sci. Total Environ.* 846, 157516. doi:10.1016/j.scitotenv.2022.157516
- Guan, Q. S., Cao, W. Z., Wang, M., Wu, G. J., Wang, F. F., Jiang, C., et al. (2018). Nitrogen loss through anaerobic ammonium oxidation coupled with iron reduction in a mangrove wetland. *Eur. J. Soil Sci.* 69 (4), 732–741. doi:10.1111/ejss.12552
- Guo, R., Chen, Y., Xiang, M., Yang, S., Wang, F., Cao, W., et al. (2024). Soil nutrients drive changes in the structure and functions of soil bacterial communities in a restored forest soil chronosequence. *Appl. Soil Ecol.* 195, 105247. doi:10.1016/j.apsoil.2023.105247
- Hardison, A. K., Algar, C. K., Giblin, A. E., and Rich, J. J. (2015). Influence of organic carbon and nitrate loading on partitioning between dissimilatory nitrate reduction to ammonium (DNRA) and N<sub>2</sub> production. *Geochimica Cosmochimica Acta* 164, 146–160. doi:10.1016/j.gca.2015.04.049
- Hazard, C., Gosling, P., van der Gast, C. J., Mitchell, D. T., Doohan, F. M., and Bending, G. D. (2013). The role of local environment and geographical distance in determining community composition of arbuscular mycorrhizal fungi at the landscape scale. *ISME J.* 7 (3), 498–508. doi:10.1038/ismej.2012.127
- Howarth, R. W., Sharpley, A., and Walker, D. (2002). Sources of nutrient pollution to coastal waters in the United States: implications for achieving coastal water quality goals. *Estuaries* 25 (4), 656–676. doi:10.1007/bf02804898
- Hu, W., Zhang, W., Zhang, L., Tong, C., Sun, Z., Chen, Y., et al. (2019). Nitrogen along the hydrological gradient of marsh sediments in a subtropical estuary: pools, processes, and fluxes. *Int. J. Environ. Res. Public Health* 16 (11), 2043. doi:10.3390/ijerph16112043
- Huang, D. Q., Fu, J. J., Li, Z. Y., Fan, N. S., and Jin, R. C. (2022). Inhibition of wastewater pollutants on the anammox process: a review. *Sci. Total Environ.* 803, 150009. doi:10.1016/j.scitotenv.2021.150009
- Huang, F., Lin, X., Hu, W., Zeng, F., He, L., and Yin, K. (2021). Nitrogen cycling processes in sediments of the Pearl River Estuary: spatial variations, controlling factors, and environmental implications. *Catena* 206, 105545. doi:10.1016/j.catena.2021.105545
- Jiang, X., Liu, C., Cai, J., Hu, Y., Shao, K., Tang, X., et al. (2023). Relationships between environmental factors and N-cycling microbes reveal the indirect effect of further eutrophication on denitrification and DNRA in shallow lakes. *Water Res.* 245, 120572. doi:10.1016/j.watres.2023.120572
- Kaden, U. S., Fuchs, E., Geyer, S., Hein, T., Horchler, P., Rupp, H., et al. (2021). Soil characteristics and hydromorphological patterns control denitrification at the floodplain scale. *Front. Earth Sci.* 9, 708707. doi:10.3389/feart.2021.708707
- Kartal, B., de Almeida, N. M., Maalcke, W. J., Op den Camp, H. J., Jetten, M. S., and Keltjens, J. T. (2013). How to make a living from anaerobic ammonium oxidation. *FEMS Microbiol. Rev.* 37 (3), 428–461. doi:10.1111/1574-6976.12014
- Kittu, L. R., Paul, A. J., Fernández-Méndez, M., Hopwood, M. J., and Riebesell, U. (2023). Coastal N<sub>2</sub> fixation rates coincide spatially with nitrogen loss in the Humboldt upwelling system off Peru. *Glob. Biogeochem. Cycles* 37 (2). doi:10.1029/2022gb007578
- Kristensen, E., Bouillon, S., Dittmar, T., and Marchand, C. (2008). Organic carbon dynamics in mangrove ecosystems: a review. *Aquat. Bot.* 89 (2), 201–219. doi:10.1016/j.aquabot.2007.12.005
- Kuypers, M. M. M., Marchant, H. K., and Kartal, B. (2018). The microbial nitrogen-cycling network. *Nat. Rev. Microbiol.* 16 (5), 263–276. doi:10.1038/nrmicro.2018.9
- La, W., Han, X., Liu, C. Q., Ding, H., Liu, M., Sun, F., et al. (2022). Sulfate concentrations affect sulfate reduction pathways and methane consumption in coastal wetlands. *Water Res.* 217, 118441. doi:10.1016/j.watres.2022.118441

- Li, X., Gao, D., Hou, L., and Liu, M. (2019a). Soil substrates rather than gene abundance dominate DNRA capacity in the *Spartina alterniflora* ecotones of estuarine and intertidal wetlands. *Plant Soil* 436 (1-2), 123–140. doi:10.1007/s11104-018-03914-w
- Li, X., Gao, D., Hou, L., Qian, W., Liu, M., Zeng, H., et al. (2021). Nitrogen loads alter the N(2) production between denitrification and anammox in Min River Estuary, a highly impacted estuary in southeast China. *Environ. Pollut.* 277, 116757. doi:10.1016/j.envpol.2021.116757
- Li, X., Wang, G., Chen, J., Zhou, X., and Liu, Y. (2022). Deciphering the concurrence of comammox, partial denitrification and anammox in a single low-oxygen mainstream nitrogen removal reactor. *Chemosphere* 305, 135409. doi:10.1016/j.chemosphere.2022.135409
- Li, Y., Bao, W., Bongers, F., Chen, B., Chen, G., Guo, K., et al. (2019b). Drivers of tree carbon storage in subtropical forests. *Sci. Total Environ.* 654, 684–693. doi:10.1016/j.scitotenv.2018.11.024
- Lin, P. (1999). *Mangrove ecosystem in China*. Beijing: Science Press.
- Luvizotto, D. M., Araujo, J. E., Silva, M. C. P., Dias, A. C. F., Kraft, B., Tegetmeyer, H., et al. (2019). The rates and players of denitrification, dissimilatory nitrate reduction to ammonia (DNRA) and anaerobic ammonia oxidation (anammox) in mangrove soils. *Acad Bras Cienc* 91 (Suppl. 1), e20180373. doi:10.1590/0001-3765201820180373
- Martiny, J. B., Bohannan, B. J., Brown, J. H., Colwell, R. K., Fuhrman, J. A., Green, J. L., et al. (2006). Microbial biogeography: putting microorganisms on the map. *Nat. Rev. Microbiol.* 4 (2), 102–112. doi:10.1038/nrmicro1341
- Melillo, J. M. (2021). Disruption of the global nitrogen cycle: a grand challenge for the twenty-first century: this article belongs to Ambio's 50th Anniversary Collection. Theme: eutrophication. *Ambio* 50 (4), 759–763. doi:10.1007/s13280-020-01429-2
- Molnar, N., Welsh, D. T., Marchand, C., Deborde, J., and Meziane, T. (2013). Impacts of shrimp farm effluent on water quality, benthic metabolism and N-dynamics in a mangrove forest (New Caledonia). *Estuar. Coast. Shelf Sci.* 117, 12–21. doi:10.1016/j.ecss.2012.07.012
- Nie, S., Zhang, Z., Mo, S., Li, J., He, S., Kashif, M., et al. (2021). Desulfobacterales stimulates nitrate reduction in the mangrove ecosystem of a subtropical gulf. *Sci. Total Environ.* 769, 144562. doi:10.1016/j.scitotenv.2020.144562
- Nogales, B., Timmis, K. N., Nedwell, D. B., and Osborn, A. M. (2002). Detection and diversity of expressed denitrification genes in estuarine sediments after reverse transcription-PCR amplification from mRNA. *Appl. Environ. Microbiol.* 68 (10), 5017–5025. doi:10.1128/AEM.68.10.5017-5025.2002
- Pan, F., Chapman, S. J., Li, Y., and Yao, H. (2017). Straw amendment to paddy soil stimulates denitrification but biochar amendment promotes anaerobic ammonia oxidation. *J. Soils Sediments* 17 (10), 2428–2437. doi:10.1007/s11368-017-1694-4
- Pandey, A., Suter, H., He, J. Z., Hu, H. W., and Chen, D. (2018). Nitrogen addition decreases dissimilatory nitrate reduction to ammonium in rice paddies. *Appl. Environ. Microbiol.* 84 (17), 008700–e918. doi:10.1128/AEM.00870-18
- Pandey, A., Suter, H., He, J.-Z., Hu, H.-W., and Chen, D. (2019). Dissimilatory nitrate reduction to ammonium dominates nitrate reduction in long-term low nitrogen fertilized rice paddies. *Soil Biol. Biochem.* 131, 149–156. doi:10.1016/j.soilbio.2019.01.007
- Pandey, C. B., Kumar, U., Kaviraj, M., Minick, K. J., Mishra, A. K., and Singh, J. S. (2020). DNRA: a short-circuit in biological N-cycling to conserve nitrogen in terrestrial ecosystems. *Sci. Total Environ.* 738, 139710. doi:10.1016/j.scitotenv.2020.139710
- Qin, J., Li, Y., Cai, Z., Li, S., Zhu, J., Zhang, F., et al. (2012). A metagenome-wide association study of gut microbiota in type 2 diabetes. *Nature* 490 (7418), 55–60. doi:10.1038/nature11450
- Qu, H. J., and Kroeze, C. (2010). Past and future trends in nutrients export by rivers to the coastal waters of China. *Sci. Total Environ.* 408 (9), 2075–2086. doi:10.1016/j.scitotenv.2009.12.015
- Raes, E. J., Karsh, K., Kessler, A. J., Cook, P. L. M., Holmes, B. H., van de Kamp, J., et al. (2020). Can we use functional genetics to predict the fate of nitrogen in estuaries? *Front. Microbiol.* 11, 1261. doi:10.3389/fmicb.2020.01261
- Rahman, M. M., Roberts, K. L., Grace, M. R., Kessler, A. J., and Cook, P. L. M. (2019). Role of organic carbon, nitrate and ferrous iron on the partitioning between denitrification and DNRA in constructed stormwater urban wetlands. *Sci. Total Environ.* 666, 608–617. doi:10.1016/j.scitotenv.2019.02.225
- Reis, C. R. G., Nardoto, G. B., and Oliveira, R. S. (2016). Global overview on nitrogen dynamics in mangroves and consequences of increasing nitrogen availability for these systems. *Plant Soil* 410 (1-2), 1–19. doi:10.1007/s11104-016-3123-7
- Rich, J. J., Arevalo, P., Chang, B. X., Devol, A. H., and Ward, B. B. (2020). Anaerobic ammonium oxidation (anammox) and denitrification in Peru margin sediments. *J. Mar. Syst.* 207, 103122. doi:10.1016/j.jmarsys.2018.09.007
- Rocca, J. D., Hall, E. K., Lennon, J. T., Evans, S. E., Waldrop, M. P., Cotner, J. B., et al. (2015). Relationships between protein-encoding gene abundance and corresponding process are commonly assumed yet rarely observed. *ISME J.* 9 (8), 1693–1699. doi:10.1038/ismej.2014.252
- Saggari, S., Jha, N., Deslippe, J., Bolan, N. S., Luo, J., Giltrap, D. L., et al. (2013). Denitrification and N<sub>2</sub>O:N<sub>2</sub> production in temperate grasslands: processes, measurements, modelling and mitigating negative impacts. *Sci. Total Environ.* 465, 173–195. doi:10.1016/j.scitotenv.2012.11.050
- Seitzinger, S. P., Kroeze, C., Bouwman, A. F., Caraco, N., Dentener, F., and Styles, R. V. (2002). Global patterns of dissolved inorganic and particulate nitrogen inputs to coastal systems: recent conditions and future projections. *Estuaries* 25 (4), 640–655. doi:10.1007/bf02804897
- Shan, J., Yang, P., Shang, X., Rahman, M. M., and Yan, X. (2018). Anaerobic ammonium oxidation and denitrification in a paddy soil as affected by temperature, pH, organic carbon, and substrates. *Biol. Fertil. Soils* 54 (3), 341–348. doi:10.1007/s00374-018-1263-z
- She, Y., Qi, X., Xin, X., He, Y., Wang, W., and Li, Z. (2023). Insights into microbial interactive mechanism regulating dissimilatory nitrate reduction processes in riparian freshwater aquaculture sediments. *Environ. Res.* 216 (Pt 2), 114593. doi:10.1016/j.envres.2022.114593
- Shen, X., Jiang, M., Lu, X., Liu, X., Liu, B., Zhang, J., et al. (2021). Aboveground biomass and its spatial distribution pattern of herbaceous marsh vegetation in China. *Sci. China Earth Sci.* 64 (7), 1115–1125. doi:10.1007/s11430-020-9778-7
- Shrewsbury, L. H., Smith, J. L., Huggins, D. R., Carpenter-Boggs, L., and Reardon, C. L. (2016). Denitrifier abundance has a greater influence on denitrification rates at larger landscape scales but is a lesser driver than environmental variables. *Soil Biol. Biochem.* 103, 221–231. doi:10.1016/j.soilbio.2016.08.016
- Song, D., Huo, T., Zhang, Z., Cheng, L., Wang, L., Ming, K., et al. (2022). Metagenomic analysis reveals the response of microbial communities and their functions in lake sediment to environmental factors. *Int. J. Environ. Res. Public Health* 19 (24), 16870. doi:10.3390/ijerph192416870
- Sun, X., Tan, E., Wang, B., Gan, Z., Yang, J., Han, J., et al. (2023). Salinity change induces distinct climate feedbacks of nitrogen removal in saline lakes. *Water Res.* 245, 120668. doi:10.1016/j.watres.2023.120668
- Tan, E., Zou, W., Jiang, X., Wan, X., Hsu, T. C., Zheng, Z., et al. (2019). Organic matter decomposition sustains sedimentary nitrogen loss in the Pearl River Estuary, China. *Sci. Total Environ.* 648, 508–517. doi:10.1016/j.scitotenv.2018.08.109
- Thamdrup, B., and Dalsgaard, T. (2002). Production of N(2) through anaerobic ammonium oxidation coupled to nitrate reduction in marine sediments. *Appl. Environ. Microbiol.* 68 (3), 1312–1318. doi:10.1128/AEM.68.3.1312-1318.2002
- Tian, M., Li, H., Wang, G., Fu, M., Qin, X., Lu, D., et al. (2023). Seasonal source identification and formation processes of marine particulate water soluble organic nitrogen over an offshore island in the East China Sea. *Sci. Total Environ.* 863, 160895. doi:10.1016/j.scitotenv.2022.160895
- Van Den Berg, E. M., Boleij, M., Kuenen, J. G., Kleerebezem, R., and Van Loosdrecht, M. C. (2016). DNRA and denitrification coexist over a broad range of acetate/N-NO<sub>3</sub><sup>-</sup> ratios, in a chemostat enrichment culture. *Front. Microbiol.* 7, 1842. doi:10.3389/fmicb.2016.01842
- Vishwakarma, S., Zhang, X., and Mueller, N. D. (2022). Projecting future nitrogen inputs: are we making the right assumptions? *Environ. Res. Lett.* 17 (5), 054035. doi:10.1088/1748-9326/ac6619
- Wang, B., and Lin, X. (2023). Exotic *Spartina alterniflora* invasion enhances sediment N-loss while reducing N retention in mangrove wetland. *Geoderma* 431, 116362. doi:10.1016/j.geoderma.2023.116362
- Wang, S., Wang, W., Zhao, S., Wang, X., Hefting, M. M., Schwark, L., et al. (2019). Anammox and denitrification separately dominate microbial N-loss in water saturated and unsaturated soils horizons of riparian zones. *Water Res.* 162, 139–150. doi:10.1016/j.watres.2019.06.052
- Wang, Y., Liu, D., Xiao, W., Zhou, P., Tian, C., Zhang, C., et al. (2021). Coastal eutrophication in China: trend, sources, and ecological effects. *Harmful Algae* 107, 102058. doi:10.1016/j.hal.2021.102058
- Wu, H. Y., Fu, S. F., Hu, W. J., Chen, F. G., Cai, X. Q., Chen, Q. H., et al. (2022). Response of different benthic biotic indices to eutrophication and sediment heavy metal pollution, in fujian coastal water, East China sea. *Chemosphere* 307 (Pt 1), 135653. doi:10.1016/j.chemosphere.2022.135653
- Xiao, M., Ding, J., Luo, Y., Zhang, H., Yu, Y., Yao, H., et al. (2022). Microplastics shape microbial communities affecting soil organic matter decomposition in paddy soil. *J. Hazard Mater* 431, 128589. doi:10.1016/j.jhazmat.2022.128589
- Xu, T., Veresoglou, S. D., Chen, Y., Rillig, M. C., Xiang, D., Ondrej, D., et al. (2016). Plant community, geographic distance and abiotic factors play different roles in predicting AMF biogeography at the regional scale in northern China. *Environ. Microbiol. Rep.* 8 (6), 1048–1057. doi:10.1111/1758-2229.12485
- Yang, X., Vancov, T., Peñuelas, J., Sardans, J., Singla, A., Alrefaei, A. F., et al. (2022). Optimal biochar application rates for mitigating global warming and increasing rice yield in a subtropical paddy field. *Exp. Agric.* 57 (5-6), 283–299. doi:10.1017/s0014479721000259
- Yao, Y., Han, B., Liu, B., Wang, Y., Su, X., Ma, L., et al. (2023). Global variations and controlling factors of anammox rates. *Glob. Chang. Biol.* 29 (13), 3622–3633. doi:10.1111/gcb.16715
- Yin, G., Hou, L., Liu, M., Liu, Z., and Gardner, W. S. (2014). A novel Membrane inlet mass spectrometer method to measure <sup>15</sup>NH<sub>4</sub><sup>+</sup> for isotope-enrichment experiments in aquatic ecosystems. *Environ. Sci. Technol.* 48 (16), 9555–9562. doi:10.1021/es501261s

- Yoon, S., Cruz-García, C., Sanford, R., Ritalahti, K. M., and Löffler, F. E. (2015). Denitrification versus respiratory ammonification: environmental controls of two competing dissimilatory NO<sub>3</sub><sup>-</sup>/NO<sub>2</sub><sup>-</sup> reduction pathways in *Shewanella loihica* strain PV-4. *ISME J.* 9 (5), 1093–1104. doi:10.1038/ismej.2014.201
- You, Q. G., Wang, J. H., Qi, G. X., Zhou, Y. M., Guo, Z. W., Shen, Y., et al. (2020). Anammox and partial denitrification coupling: a review. *RSC Adv.* 10 (21), 12554–12572. doi:10.1039/d0ra00001a
- Yu, H., Liu, X., Yang, C., Peng, Y., Yu, X., Gu, H., et al. (2021). Co-symbiosis of arbuscular mycorrhizal fungi (AMF) and diazotrophs promote biological nitrogen fixation in mangrove ecosystems. *Soil Biol. Biochem.* 161, 108382. doi:10.1016/j.soilbio.2021.108382
- Zhang, N., Guo, R., Wang, F., Dai, Z., Li, Y., and Cao, W. (2023). Warming tends to promote nitrogen conservation but stimulate N<sub>2</sub>O emissions in mangrove sediments. *Ecosystems* 27, 235–249. doi:10.1007/s10021-023-00885-7
- Zhang, S., Qin, W., Bai, Y., Zhang, Z., Wang, J., Gao, H., et al. (2020). Linkages between anammox and denitrifying bacterial communities and nitrogen loss rates in high-elevation rivers. *Limnol. Oceanogr.* 66 (3), 765–778. doi:10.1002/lno.11641
- Zhao, J., Yang, Y., Xu, H., Zheng, J., Shen, C., Chen, T., et al. (2023). Data-independent acquisition boosts quantitative metaproteomics for deep characterization of gut microbiota. *NPJ Biofilms Microbiomes* 9 (1), 4. doi:10.1038/s41522-023-00373-9